Alternating Wet and Dry Conditions over South America during Summer

JULIA NOGUÉS-PAEGLE

Department of Meteorology, University of Utah, Salt Lake City, Utah

KINGTSE C. MO

NCEP/NOAA, Washington, D.C.

(Manuscript received 5 March 1996, in final form 17 June 1996)

ABSTRACT

Time series of outgoing longwave radiation (OLR) fields and various gridded reanalysis products are used to identify and describe periods with abundant and deficient rainfall over South America during summer. Empirical orthogonal function analyses of OLR anomalies filtered to retain variations longer than 10 days reveal a meridional seesaw of dry and wet conditions over tropical and subtropical South America. It appears that intensification of the South Atlantic convergence zone (SACZ) is associated with rainfall deficits over the subtropical plains of South America. In contrast, when the SACZ weakens, precipitation over these plains is abundant. These results are in agreement with those of Kousky and Casarin.

This seesaw pattern appears to be a regional component of a larger-scale system, possibly related to the 30–60-day oscillation in the Tropics, with the southward extension and strengthening of the SACZ found with enhanced tropical convection over the central and eastern Pacific and dry conditions over the western Pacific and the Maritime Continent. At the same time, convection is suppressed in the region of the South Pacific convergence zone, over the Gulf of Mexico, and in the ITCZ over the North Atlantic.

In the opposite phase there is a strong influx of moisture from the Tropics into central Argentina and southern Brazil. The moisture influx is enhanced by a strong low-level jet (LLJ) east of the Andes. The LLJ displays a marked diurnal oscillation and characteristics similar to the well-documented LLJs over the Great Plains of North America.

1. Introduction

The subtropical plains of South America exhibit precipitation and temperature regimes that are conducive to plentiful harvests and are therefore important sources of regional food supplies. Climate variations of this region carry important practical economic and social consequences, and this has prompted some past studies of rainfall and moisture budget climatologies. For example, Kousky and Casarin (1986) have related periods of deficient rainfall over southern Brazil with enhanced rainfall over the Atlantic. Buchmann et al. (1990) have performed real-data global model integrations that support this correlation on timescales as short as 10 days. Berri and Inzunza (1993) and Wang and Paegle (1996) investigated moisture budgets over this region and demonstrate substantial moisture flux by the low-level jet (LLJ).

Each of the aforementioned studies focused on particular aspects of the regional circulation using limited periods and datasets, but they have not computed moisture fluxes within different rainfall regimes. The central goal of the present study is to further pursue these lines of research using more extensive global analyses and statistical methods with an emphasis upon regional and larger-scale correlations with the South Atlantic convergence zone (SACZ). Enhanced and suppressed convection over the SACZ are associated with distinct differences in moisture transport and rainfall over subtropical South America and display associated anomalies westward into the Pacific Ocean.

Figure 1 displays the climatological precipitation pattern over South America averaged from December to March using station rainfall data over land and MSU (Microwave Sounding Unit) precipitation estimates over the oceans (Schemm et al. 1992). There are two well-defined precipitation bands: one extends from tropical South America toward the northeast and the other toward the southeast. The first one is located close to the equator and is a component of the ITCZ. The second band is referred to as the South Atlantic convergence zone, and it is a typical feature of South American summers. Large-scale circulations associated with the SACZ

Corresponding author address: Dr. Julia Nogues-Paegle, Dept. of Meteorology, University of Utah, 819 Wm. C. Browning Bldg, Salt Lake City, UT 84112.
E-mail: jnpaegle@atmos.met.utah.edu

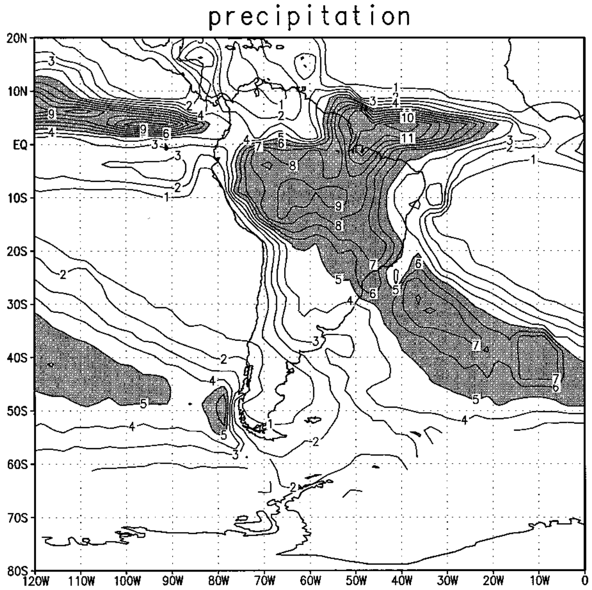

FIG. 1. Monthly mean total precipitation averaged from December through March 1979–93, contoured every 1 mm day^{-1}.

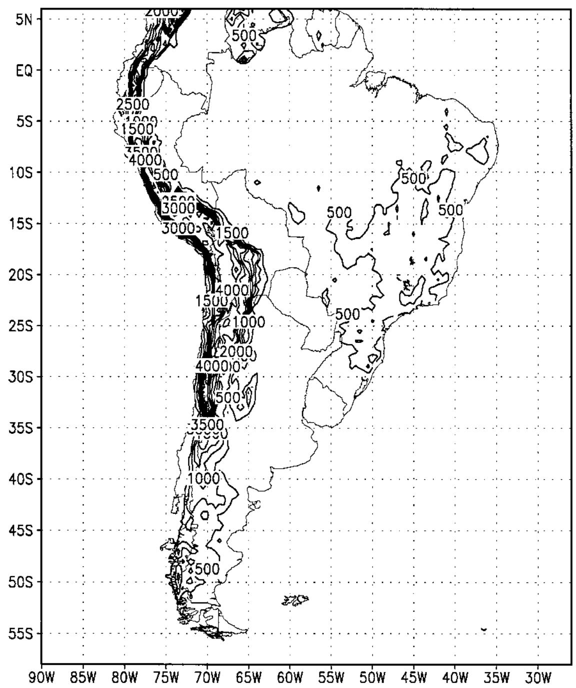

FIG. 2. Terrain elevation contoured every 500 m.

are influenced by local heating and orography and are connected to the tropical intraseasonal oscillation.

Figure 2 shows the South American orography as resolved with a 0.5° grid. This orography, in association with a large landmass in tropical latitudes, provides a unique environment for development of monsoonal circulations with heavy summer rains centered at 10°S, as shown on Fig. 1. The Bolivian Plateau, which is widest at about 18°S, serves as an elevated source of sensible heat, but the latent heating released from organized convection is the largest contributor to the heat source over South America (e.g., Rao and Ergodan 1989).

The effect of tropical topography has been discussed by Meehl (1992) who notes its dual effect in 1) disturbing the prevailing zonal flow and 2) intensifying the land–sea temperature contrast through an elevated heat source with local rising motion, rainfall, and associated release of latent heat. Monsoonal circulations over South America are similar to those over North America and Asia in exhibiting characteristics of a giant land–sea breeze, with heavy summer precipitation, an upper-level anticyclone (the Bolivian high), a low-level trough, and intensification of the subtropical jet.

The summer circulation over South America has been qualitatively reproduced as the response to transient tropical convection (Silva Dias et al. 1983) using a linear model similar to that of Gill (1980). Resulting features in this model include the Bolivian high, which suggests that this high pressure system may be more a result of the tropical convection than the elevated heat source. Orographic effects (Kleeman 1989; Gandu and Geisler 1991) and an active diurnal cycle (Figueroa et al. 1995) appear to be necessary to obtain a realistic description of the SACZ. Nevertheless, the sparse network of conventional observations over South America has made it difficult to ascertain the extent to which model results realistically simulate atmospheric conditions over the region. The recent availability of reanalyses produced with retrospective analyses of conventional and satellite observations by current global assimilation systems allows documentation of the three-dimensional circulations over South America for extended periods. Furthermore, reanalysis products are archived every 6 h allowing quantification of diurnal oscillations. The extent to which such oscillations are observed in the atmosphere remains to be determined since the frequency of synoptic observations is not high enough to adequately resolve diurnal cycles. It has been recently determined that the Australian surface analyses used as ''bogus'' in the Southern Hemisphere to increment surface pressure data over the oceans were not correctly assimilated in the reanalyses produced by a joint effort between the National Centers for Environmental Prediction and the National Center for Atmospheric Research (NCEP–NCAR reanalysis project). These reanalyses are used in this study. The overall effect of this error in the gridded analyses is minor (E. Kalnay 1996, personal communication). Nevertheless, main features reported in this paper were also found in the reanalyses produced by the Data Assimilation Office of the National Aeronautics and Space Administration Goddard Space Flight Center (DAO/NASA reanalysis) confirming that results presented here are not dependent on the reanalysis system used.

Intraseasonal variations of South American summer circulations have been associated with the 30–60-day

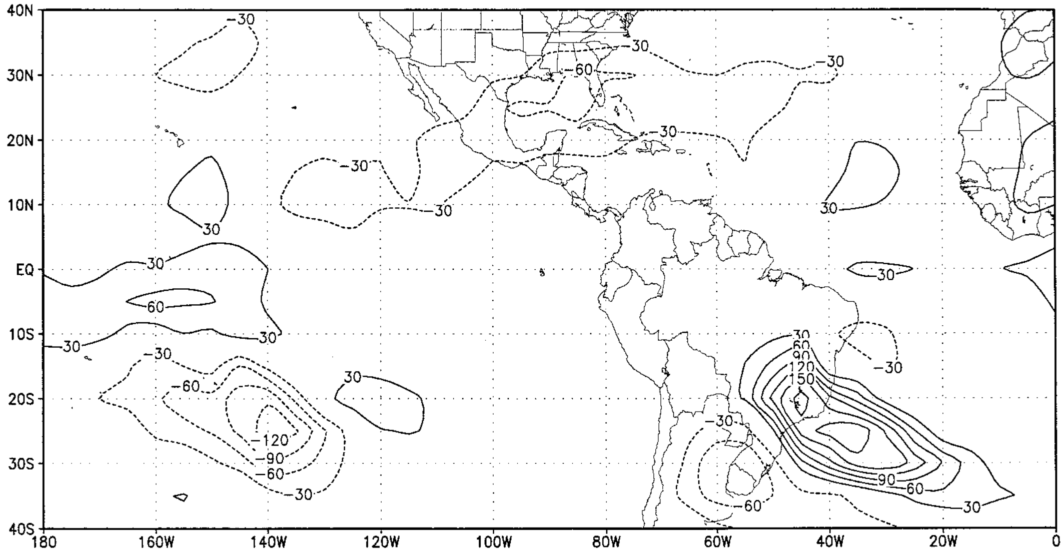

FIG. 3. REOF 5 pattern for the intraseasonal filtered OLR anomalies contoured every 30 nondimensional units.

(Madden–Julian) oscillation by Kousky and Kayano (1994) and Park and Schubert (1993). Additionally, Kousky and Casarin (1986) used half-monthly means of outgoing longwave radiation (OLR) anomalies and 200-hPa winds to relate deficient rainfall over southern Brazil with an enhancement of the SACZ. There appears to be a north–south seasaw of the SACZ precipitation band, producing wet conditions over the subtropical latitudes when the SACZ is weak. These studies are extended here using daily OLR values filtered to retain a broad band of low-frequency variations (10–90-day periods). The timescale of the SACZ seasaw pattern is identified through composites lagged from times of enhanced and suppressed convection over the SACZ. NCEP–NCAR reanalyses (Kalnay et al. 1996) are used to describe the three-dimensional structure of atmospheric motions and its evolution from dry to wet periods over southern Brazil and central Argentina. In particular, LLJs east of the Andes and their role in transporting moisture from the Amazon Basin into the South American subtropical plains are discussed.

The paper is structured as follows: section 2 describes data and methods used, section 3 discusses the composite structure of the seasaw patterns referred to above, and section 4 examines a case study during February and March 1987, when an episode of wet conditions over central Argentina and Uruguay was followed by dry weather with a concomitant enhancement of the SACZ. Section 5 summarizes results and conclusions.

2. Data and methodology

a. Data

Daily OLR data from 1 June 1974 to 31 June 1993 (with 10 months missing in 1978) are used as proxies of tropical convection. This dataset has been interpolated to remove gaps due to missing values. The source dataset was obtained from National Environmental Satellite, Data, and Information System averages of individual satellite scans onto 2.5° grids. The daily values represent averages of the day and night passes of the polar-orbiting satellites (Liebmann and Smith 1996).

Gridded global analyses available on a 2.5° × 2.5° latitude–longitude grid and every 6 h from the NCEP–NCAR reanalyses from 1982 to 1993 are used to represent atmospheric conditions and to quantify diurnal variations. The period 15 November–15 March is taken to be representative of austral summer. There are 28 sigma levels in the assimilation model (Kalnay et al. 1996) with 8 levels at or below 800 hPa (0.80, 0.84, 0.88, 0.915, 0.942, 0.964, 0.982, and 0.995). This gives a good resolution of moisture transport within the lowest layers of the atmosphere. The precipitation is accumulated from the 6-h forecast cycle. The evaluation of forecast products and moisture transport can be found in Mo and Higgins (1996).

The DAO/NASA reanalysis data from 1 March 1985 to November 1993 are also used. The DAO data assimilation system is described by Schubert et al. (1993). Their model, referred to as the Goddard Earth Observing System (GEOS), model has a resolution of 2° latitude by 2.5° longitude on a staggered C grid (Mesinger and Arakawa 1976). There are 20 sigma levels with 4 levels below 850 hPa. A three-dimensional multivariate optimal interpolation scheme (Pfaendtner et al. 1995) is used. One major difference between the two models is in the parameterization of convection. The NCEP model uses an improved version of the Pan–Grell scheme (Pan and Wu 1993), while the GEOS model uses the relaxed Arakawa–Schubert scheme developed by Moorthi and Suarez (1992). A simple biosphere model (Sellers et al. 1986) is included in the NCEP model. Soil moisture in

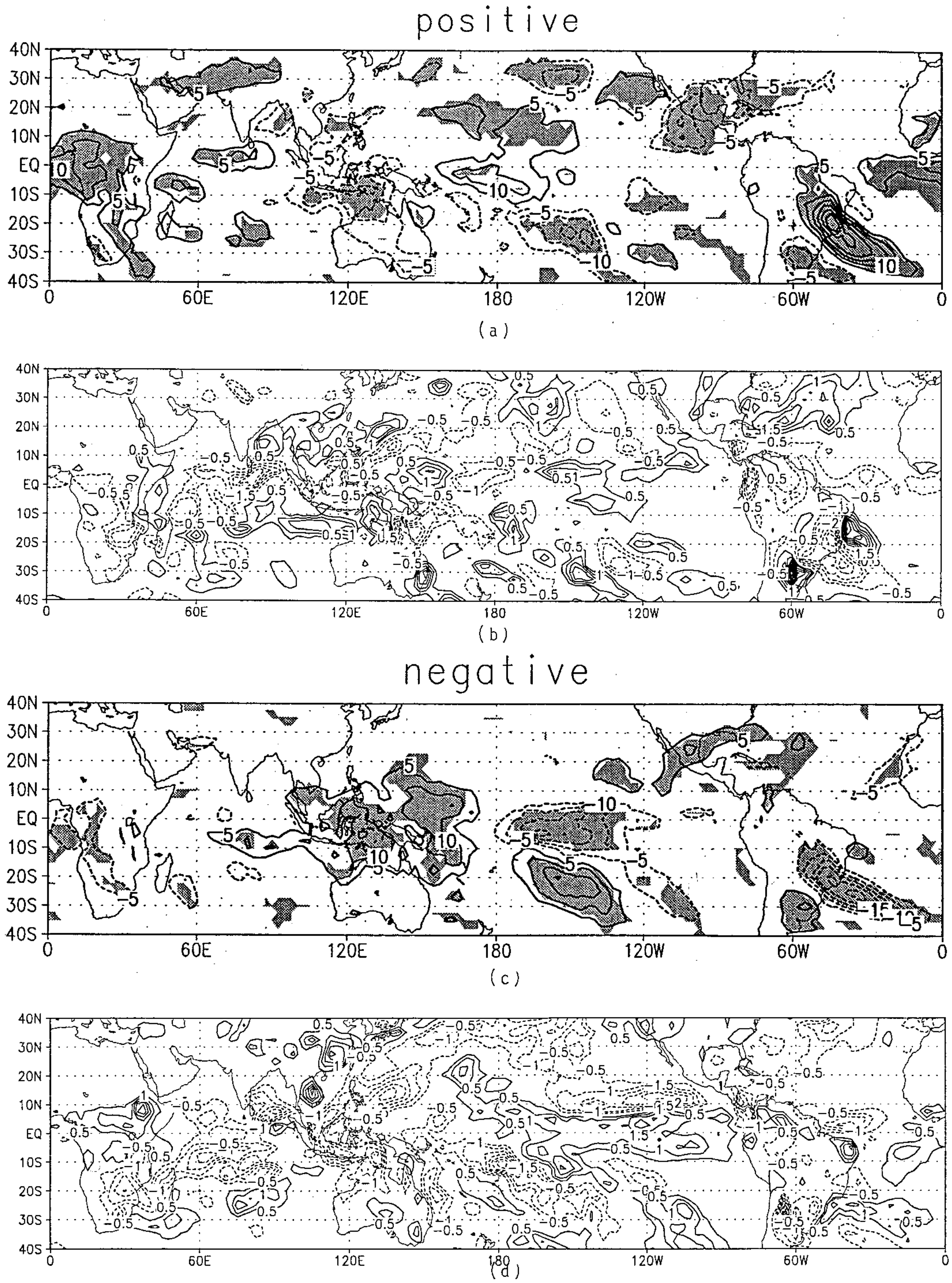

FIG. 4. Composites for SACZ positive events of (a) OLR anomalies contoured every 5 W m^{-2} and (b) rainfall anomalies contoured every 0.5 mm day^{-1}. Zero contours are omitted, and shading indicates statistical significance at the 95% level. (c) Same as (a), and (d) same as (b) but for the negative case.

the GEOS model is obtained with a simple bucket model using monthly mean observed surface air temperature and precipitation (Schemm et al. 1992). The DAO/NASA assimilation system also includes an incremental analysis update procedure (Bloom et al. 1991), which greatly reduces initial imbalances and spinup and eliminates shocks due to the insertion of input data. The increments are constant over the 6-h period centered on the output times, and they are consistent with the diagnostic quantities based on 6-h averages from the NCEP.

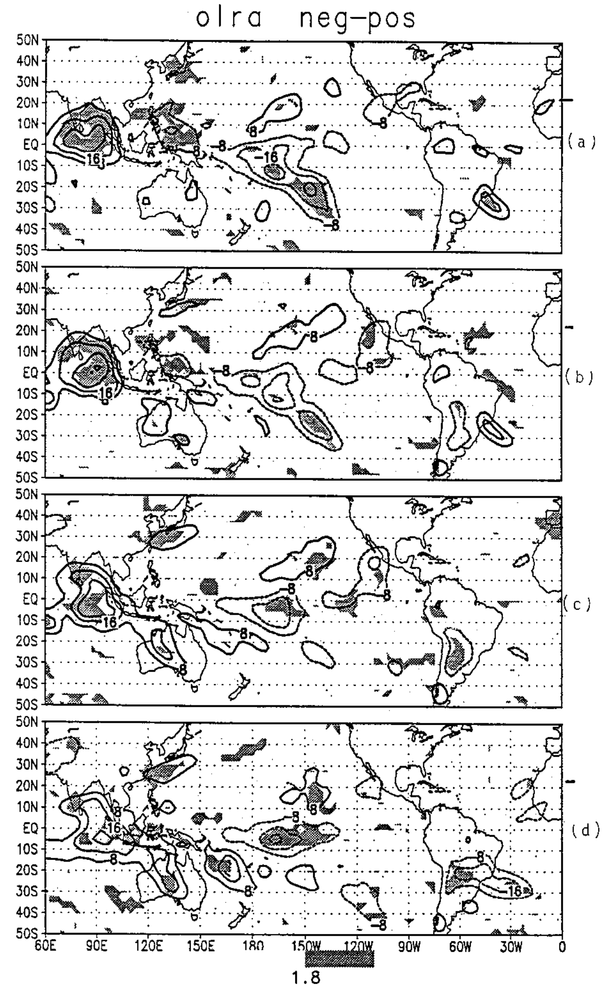

FIG. 5. OLRA composite difference between negative and positive events for the SACZ for the pentad centered (a) day −8, (b) day −6, (c) day −4, and (d) day −2 from the onset of a SACZ event. Contour interval is 8 W m^{-2}. Zero contours are omitted; 95% statistically significant areas are shaded.

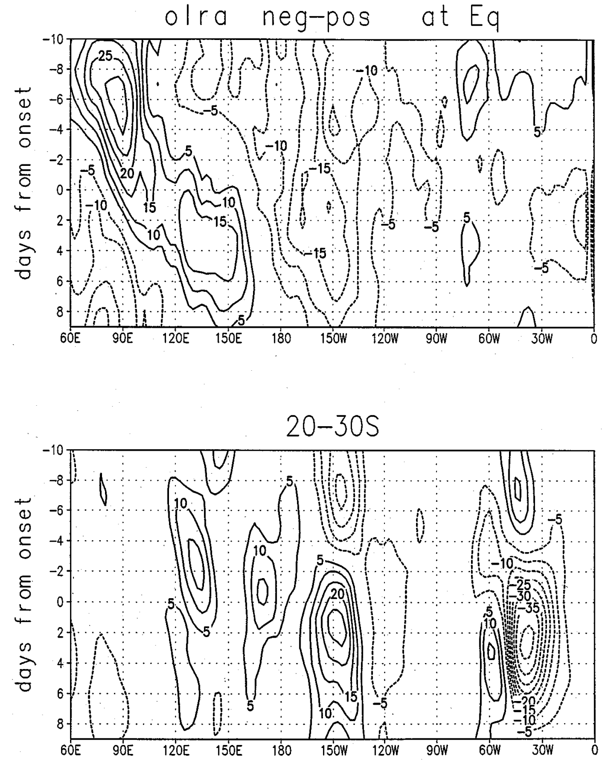

FIG. 6. OLRA composite difference between negative and positive events (top) at the equator (bottom) averaged between 20° and 30°S. Nonzero values are contoured every 5 W m^{-2}.

b. Methodology

The seasonal cycle is defined as the sum of annual and semiannual cycles and a grand mean. Anomalies are defined as differences between daily values and the seasonal cycle, and OLR anomalies were filtered to retain fluctuations with periods between 10 and 90 days. The seasonal cycle was defined using all available data for each dataset.

Empirical orthogonal function analysis was performed on the intraseasonal filtered OLR pentad anomalies from 1974/75 to 1992/93. The domain covers the area identified by the Pan American Climate Studies program (40°S–40°N, 180°–20°E). To avoid degeneracy, rotated EOFs were obtained using the varimax rotation method (Richman 1986; Richman and Lamb 1985). The number of eigenmodes to be rotated was based on the criterion given by O'Lenic and Livezey (1988). Computations were done for three datasets: 1) includes warm and cold phases of El Niño–Southern Oscillation (ENSO) events, 2) consists of the complementary non-ENSO years, and 3) is the total dataset. The ENSO years are chosen as 1976/77, 1982/83, 1983/84, 1986/87, 1988/89, and 1991/92 and the remaining years are considered as non-ENSO years.

3. Seesaw of precipitation regimes over South America

Rotated EOF 5 for the ENSO years depicts a well-marked SACZ (Fig. 3) and explains 3.8% of the variance. A similar pattern appears as REOF 11 in the nonstratified dataset, suggesting that the SACZ is modulated by ENSO. Figure 3 implies that a weak SACZ (positive OLR loadings) is accompanied by enhanced rainfall (negative loadings) over the Gulf of Mexico and over northern Argentina and southern Brazil. The interpretation that low OLR values result in increased precipitation should be exercised with caution over the subtropics of the winter hemipshere since cirrus and other nonprecipitating clouds may result in negative OLR anomalies. Positive and negative events associated with SACZ OLR variations are selected next.

The intraseasonal filtered OLR anomalies were projected onto REOF 5 to obtain principal component (PC)

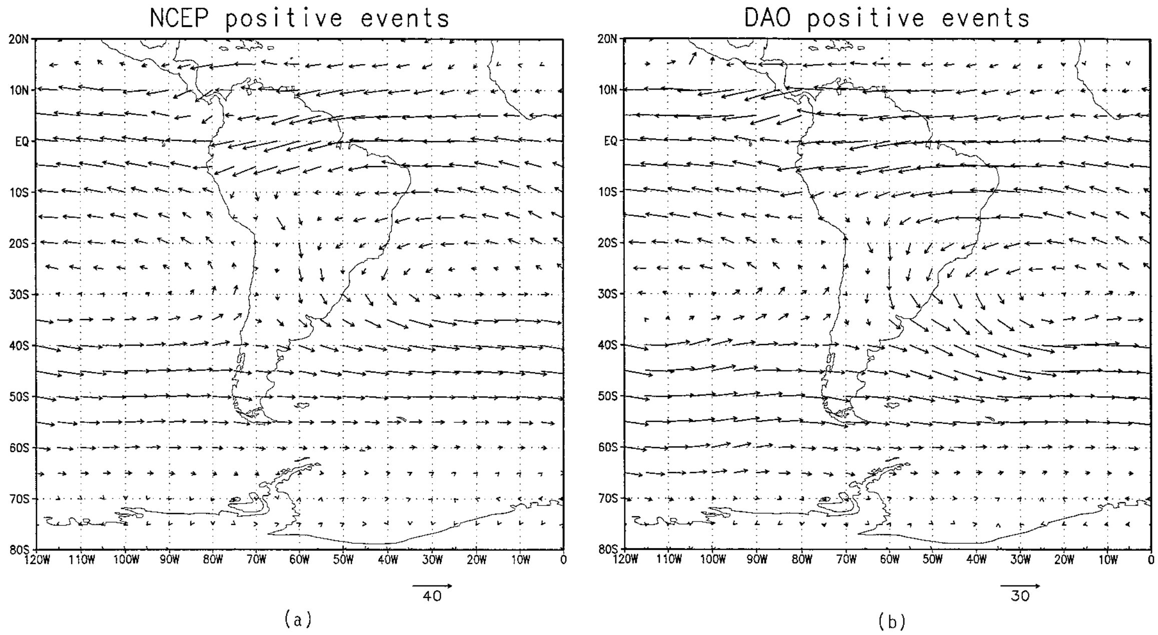

FIG. 7. Vertically integrated moisture flux composite for positive events for (a) the NCEP–NCAR and (b) DAO/NASA reanalyses. Units are 100 g cm^{-1} s^{-1}.

5. The standard deviation of PC 5 was computed using all 18 summer seasons. Positive (negative) events were chosen when PC 5 was greater (smaller) than a threshold for more than 5 consecutive days. The threshold is chosen as 1.2 of its own standard deviation. The duration of an event is defined from the time when PC 5 first crosses the threshold (onset) to the time when the next crossing of the threshold (demise) occurs. Increased convection in the SACZ is therefore found in the negative phase when the OLR values are small and give negative loadings in the EOF analysis. From 1974 to 1993, there are 28 positive events with 14 events during 6 ENSO years and 14 events during the remaining 12 years. There are 34 negative events with 22 events during ENSO and 12 during the non-ENSO years. This pattern is three times more likely to occur during ENSO for the period considered here. The average duration is 7.14 days for the positive events and 7.84 days for the

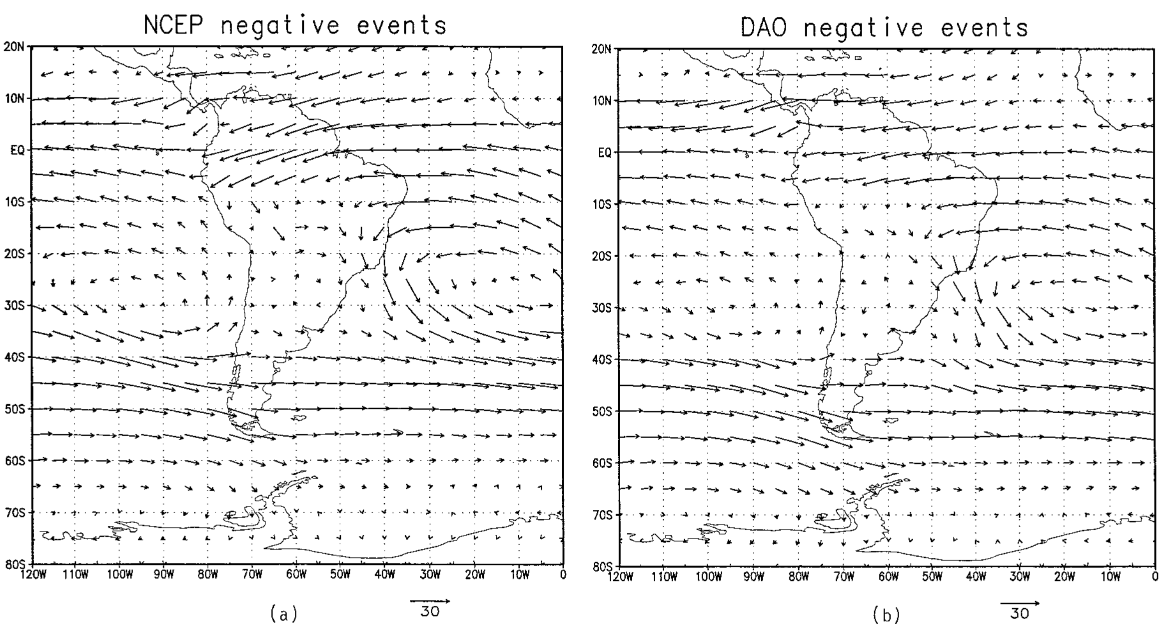

FIG. 8. Same as Fig. 7 but for negative events.

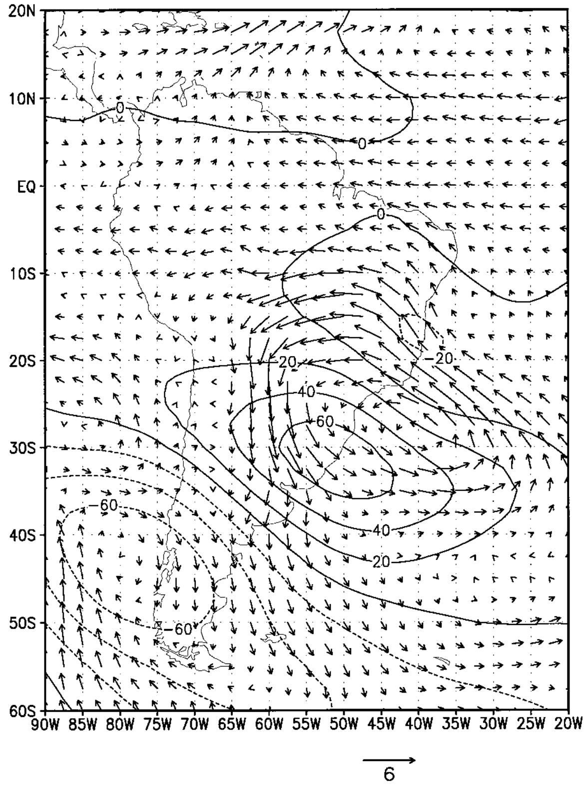

FIG. 9. The 200-hPa height difference (contour) and 850-hPa wind difference (arrow) between positive and negative events from the NCEP–NCAR reanalysis. Contour interval is 10 m, and the maximum wind vector is 10 m s^{-1}.

negative events. Detailed studies to examine the ENSO modulation of the SACZ will be conducted when the 40-year reanalysis is completed.

For each event, mean OLR anomalies were computed by averaging over the duration of that event, and the OLR anomaly composites were obtained by averaging over all events. The shading in subsequent diagrams indicates areas where the value is statistically significant at the 95% level by assuming one degree of freedom per event. OLRA composites for positive (Fig. 4a) and negative events (Fig. 4c) are nearly opposite images of each other, and that increases the confidence in the signal. The southward extension and strengthening of the SACZ are associated with enhanced tropical convection in the central and eastern Pacific and dry conditions in the western Pacific and the Maritime Continent. The South Pacific convergence zone (SPCZ) is suppressed as well as the ITCZ through the Gulf of Mexico to the Atlantic. Precipitation anomaly composites computed from NCEP reanalysis rainfall estimates are shown in Figs. 4b and 4d. The southward extension and strengthening of the SACZ for the negative phase are associated with suppressed rainfall from 20°–40°S to 50°–70°W. The opposite is true for the positive phase, which also shows enhanced rainfall off the coast of Brazil between 10° and 20°S, and maximum rainfall anomalies up to 3 mm day^{-1} over northern Argentina and southern Brazil.

The evolution of the seesaw pattern over South America (henceforth referred to as the SASS for South America seesaw) is documented in Fig. 5, which depicts composites of OLR anomaly differences between negative and positive events. Statistically significant areas (95% level) are shaded by assuming one degree of freedom per event. The southward extension and strengthening of the SACZ are associated with enhanced tropical convection in the central Pacific Ocean. OLR anomalies exhibit an eastward propagation of approximately 5° day^{-1} at equatorial latitudes (Fig. 6, top). Farther south, between 20° and 30°S, OLR anomalies exhibit a standing pattern between 60° and 40°W (Fig. 6, bottom). This suggests a role for the South American continent in locking the convective anomalies at these longitudes. Subtropical OLR anomalies at about 150°W display an opposite sign to those found 90° eastward. Figures 5 and 6 give a timescale of about 10 days for the SASS to complete a half-cycle (from the positive to the negative phase) and links its evolution to convection over the Pacific Ocean. Figure 5 also shows dry conditions in the western Pacific and the Maritime Continent associated with a strengthened SACZ. The SPCZ is also suppressed at this time.

The positive rainfall anomalies over the South American subtropics are supported by a northerly vertically integrated moisture flux shown in Fig. 7. The Andes deflect low-level wind currents and create strong convergence of moisture flux at about 35°S. It may be argued that the moisture flux shown here is to a certain extent a reflection of data assimilation model design. Figure 7b shows moisture flux composites obtained from the DAO/NASA assimilation system, and Fig. 8 displays similar computations for the negative phase. The SASS is well represented in both analyses, which show a strong northerly moisture flux at about 35°S, 60°W for the positive phase, with an eastward shift to about 40°W during the negative phase. The northerly moisture flux rotates into the westerly current at about 40°S, with the DAO/NASA analyses giving a stronger meridional flux onto higher latitudes for both extremes of the SASS. Differences between the analyses are also apparent in the easterly moisture flux from the Atlantic Ocean into central Brazil, with a stronger northeasterly component in the NCEP–NCAR reanalysis for both composites. Nevertheless, the main feature of importance to the SASS, namely the eastward shift of the subtropical high as the SASS proceeds from its positive to negative phase, is evident in both reanalysis products.

The analysis difference of vertically integrated moisture flux results mostly from low-level winds as shown in Fig. 9, rather than from specific humidity differences as documented by Wang and Paegle (1996). Figure 9 depicts wind differences at 850 hPa and height differences at 200 hPa between both phases of the SASS. It is evident that the strong low-level northerlies at about

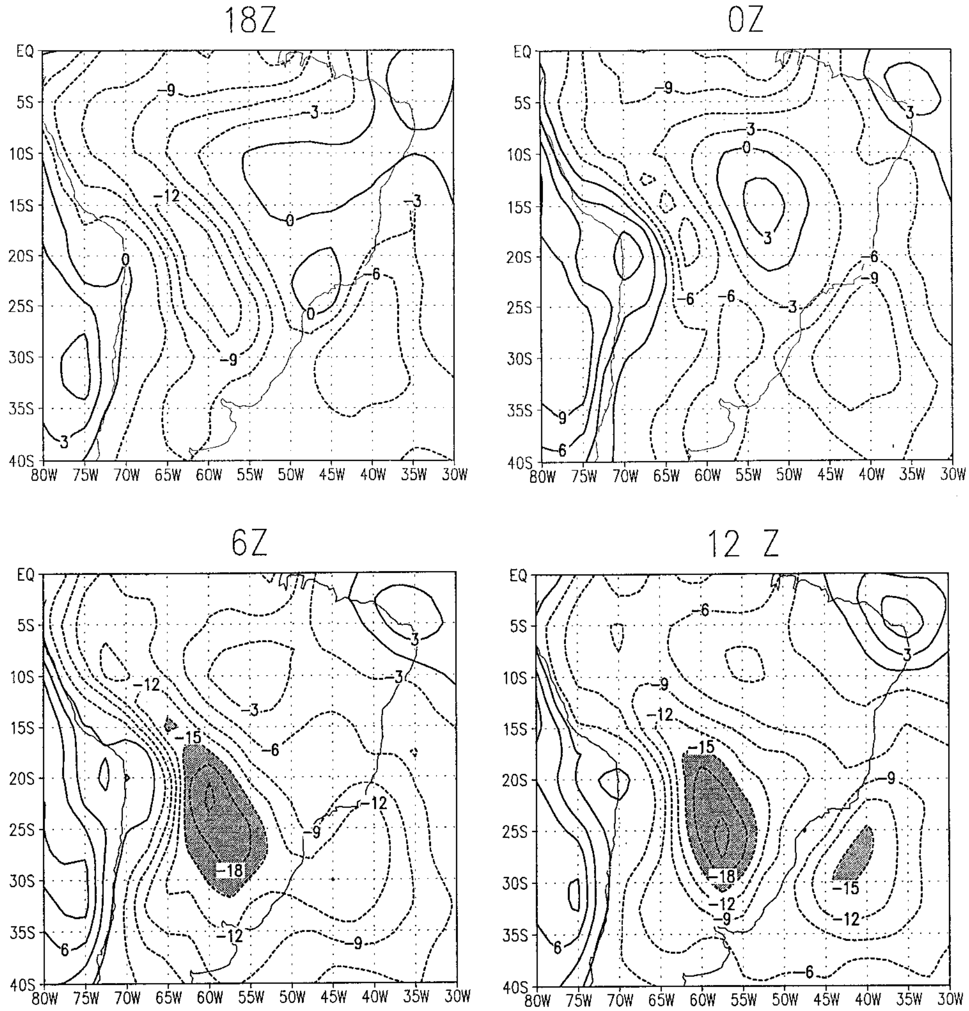

FIG. 10. Vertically integrated meridional moisture flux composite for the positive phase at 1800, 0000, 0600, and 1200 UTC as labeled in the figure from the NCEP–NCAR reanalysis. Contour interval is 300 g cm^{-1} s^{-1}.

30°S over the continent are associated with a westward displacement of the subtropical high and lower 200-hPa heights to the southwest for the positive phase relative to the negative phase. The 200-hPa height field shows a well-defined wave pattern with a wavelength of about 70° longitude.

The meridional component of the vertically integrated moisture flux has a strong diurnal cycle, as shown in Fig. 10 for the positive phase, with maximum values found between 0600 and 1200 UTC (0200 and 0800 local time). The strong diurnal modulation of the vertically integrated moisture flux is due to a diurnally oscillating low-level jet. This is illustrated next for a case study during summer 1987.

4. Case study

A time series of PC 5 (not shown) reveals that the period 21 February–2 March 1987 was in a positive SASS phase and a negative phase followed during 7–14 March. These periods are chosen for the case study. Figure 11a shows a well-defined SACZ in the NCEP–NCAR reanalysis estimates of precipitation for the 7–14 March period. The difference in precipitation (Fig. 11b) between this period and that of the positive phase reveals enhanced rainfall at about 25°S in the SACZ and diminished precipitation in longitudinally elongated bands flanking the 20°–30°S band. Enhanced convection in the SACZ occurs with below normal upper-tropospheric heights centered at approximately 45°W and above normal tropospheric heights entering the South American continent off the coast of Chile (Fig. 11c). This pattern is reversed for the positive phase, when enhanced precipitation over the continent at 35°S is found associated with below normal heights off the west coast. A similar circulation reversal was noted in the composite circulations.

The meridional moisture flux (Fig. 12) maximizes

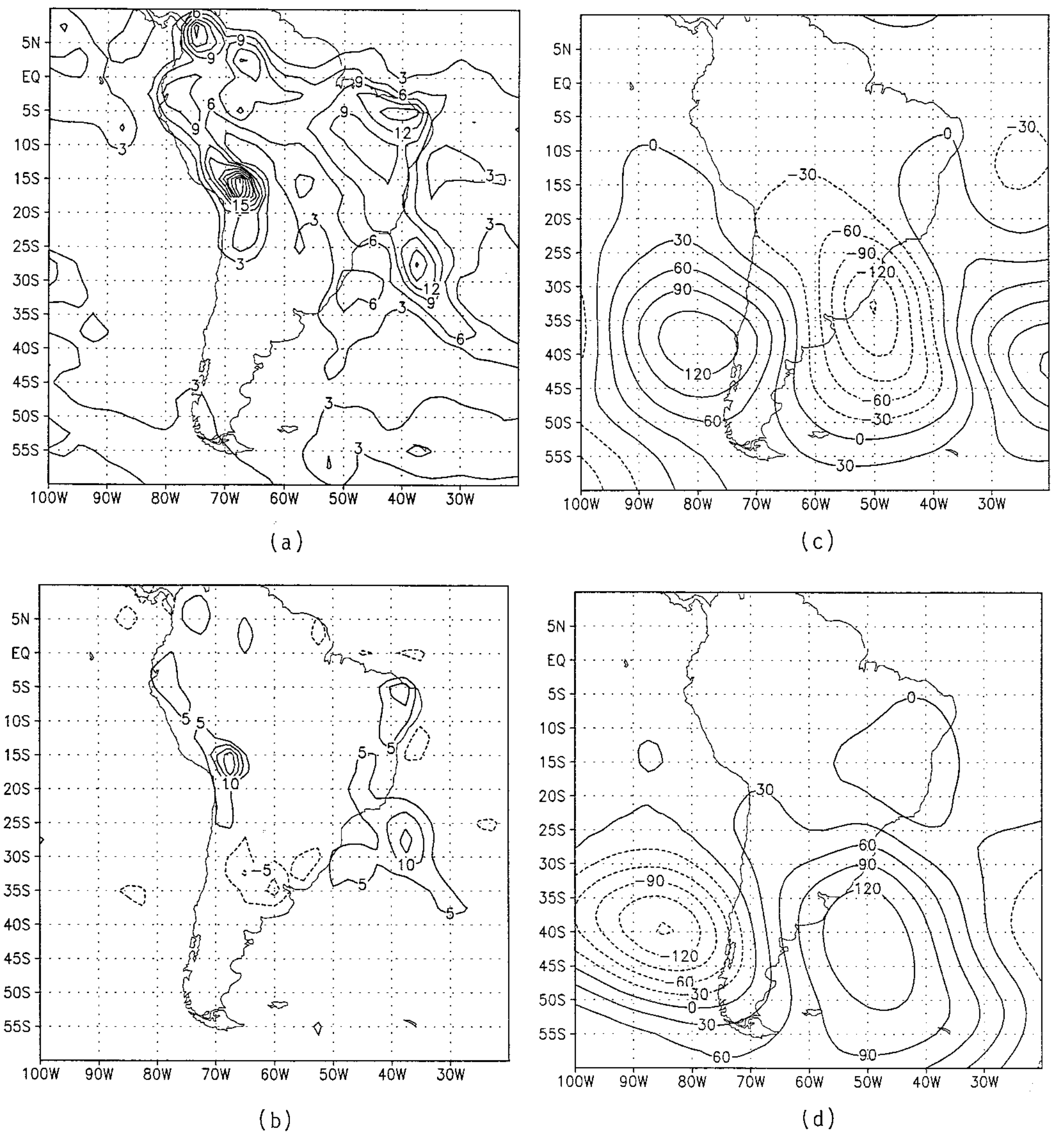

FIG. 11. (a) Precipitation averaged between 7 and 14 March 1987. Contour interval is 2 mm day^{-1}. (b) Precipitation difference between the period from 7 to 14 March 1987 and the period 21 February–2 March 1987. Contour interval is 2 mm day^{-1}. (c) The 200-hPa height difference between the mean from 7 March to 14 March 1987 and the mean for the study period from 1 February to 30 March 1987, contoured every 30 m. (d) Same as (c) but for the period 21 February–2 March 1987.

from 0600 to 1200 UTC (0200–0800 local time at 60°W) as in the case of the composite phase. Figure 13 compares the vertically integrated meridional moisture flux for the period 21 February–2 March as given by the NCEP–NCAR analysis with that from the DAO/NASA analyses. Though some differences are evident, the two estimates are roughly in agreement with maximum negative values found over northern Argentina and southeastern Brazil.

Figure 14 (top) displays a longitude–time diagram of the meridional wind component at 27.5°S where the maximum meridional moisture flux is found east of the Andes in the NCEP–NCAR reanalysis. The diagram shows a diurnally oscillating wind with maximum oscillation amplitude at 57.5°W, the longitude of maximum meridional moisture flux, indicating that most of this moisture flux is accounted for by the low-level winds. The height–time cross section (Fig. 14, bottom) indicates that the maximum oscillation amplitude is found at 925 hPa (about 500 m above ground). The oscillation amplitude decays as the northerlies shift to southerlies in association with the SACZ enhancement.

The latitude of maximum low-level meridional wind is close to 30°S, and it is therefore tempting to relate the northerly jet observed for the positive phase of the SASS with a diurnally varying forcing. A simple linear

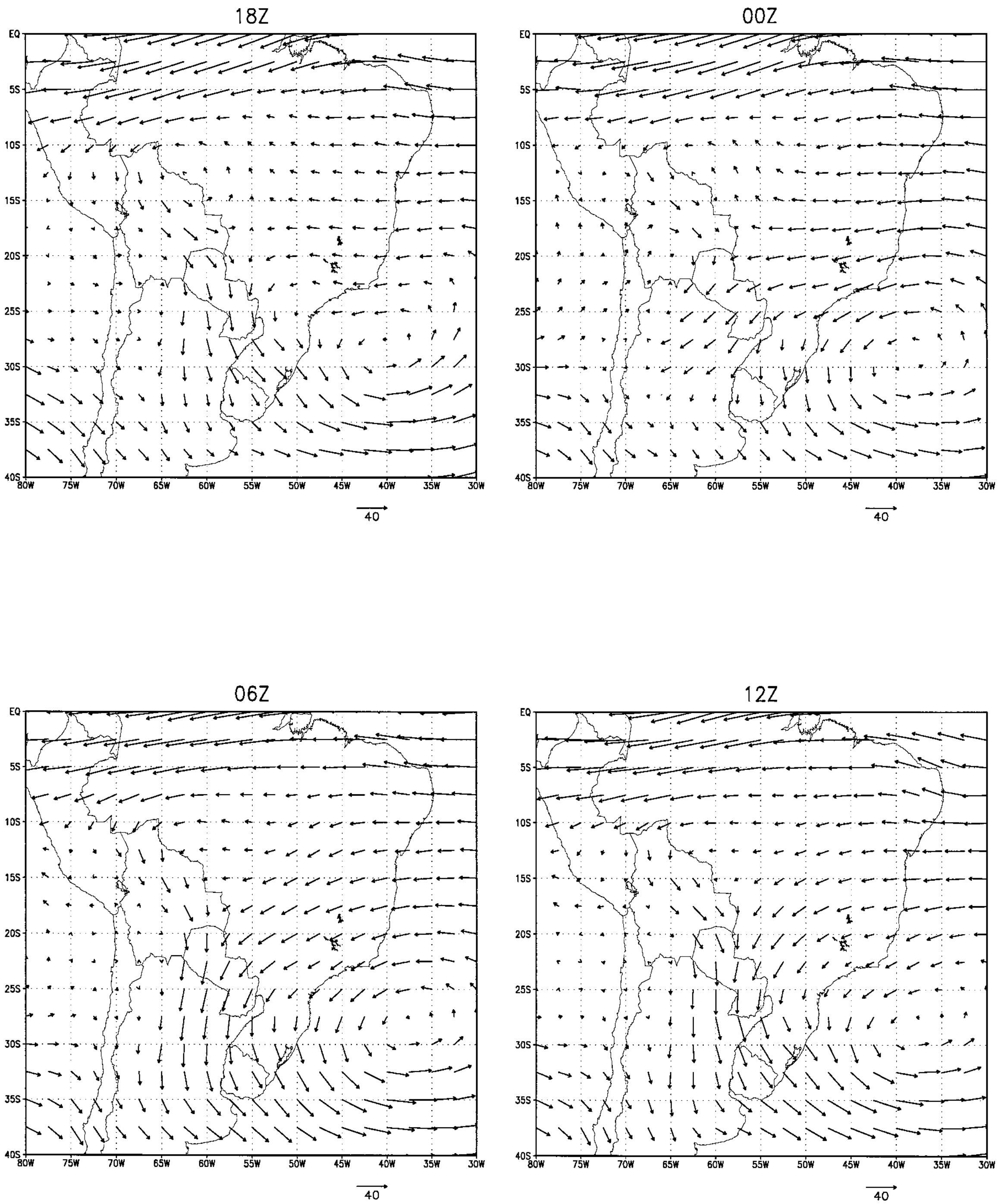

FIG. 12. Vertically integrated moisture flux averaged from 21 February to 2 March 1987 for 1800, 0600, 0000, and 1200 UTC; units are 100 g cm^{-1} s^{-1} from the NCEP–NCAR reanalysis.

interpretation is offered next for slope-driven circulations around north–south-oriented mountains (such as the Andes). In this case, a diurnally oscillating buoyancy forcing is mostly found in the longitudinal direction and it is imposed here through an $A\cos(\omega t)$ function, where ω is the diurnal frequency. The linear momentum equations are

$$\frac{\partial u}{\partial t} = fv = A\cos(\omega t) - Ku \tag{1}$$

and

$$\frac{\partial v}{\partial t} + fu = -Kv, \tag{2}$$

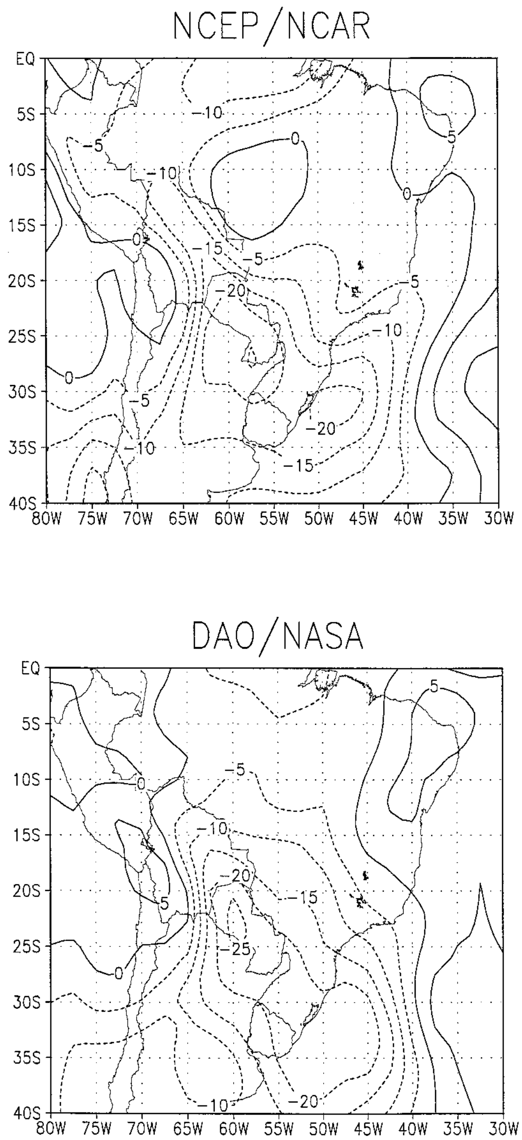

FIG. 13. Vertically integrated meridional moisture flux averaged from 21 February to 2 March 1987 for the NCEP–NCAR and DAO/NASA reanalyses. Contour interval is 500 g cm^{-1} s^{-1}.

where u and v are the zonal and meridional wind components, K is a Newtonian drag coefficient, and the Coriolis parameter is given by

$$f = 2\omega \sin\phi.$$

Equations (1) and (2) may be combined in a single linear equation given by

$$\frac{\partial(u + iv)}{\partial t} + if(u + iv) = A\cos(\omega t) - K(u + iv). \tag{3}$$

The solution to this equation is

$$(u + iv) = \frac{1}{4}\left[\frac{Ae^{i\omega t}}{i(\omega + f) + K} + \frac{Ae^{-i\omega t}}{i(-\omega + f) + K}\right]. \tag{4}$$

At 30°, the forcing frequency coincides with the Coriolis parameter, giving an amplified diurnally oscillating response that also depends on the amplitude of the forcing. The present simple model only includes the influence of buoyancy oscillations above sloping terrain. This mechanism was first studied analytically by Holton (1967) in an effort to explain the diurnal oscillations of the Great Plains low-level jet of North America. This and other mechanisms, such as diurnal oscillations of turbulent mixing and of stratification and related flow blocking, are sometimes used to explain the strong diurnal cycle of low-level winds found east of the Rocky Mountains of North America. Each of these theories has the common feature that they predict strongest response at 30° latitude where the natural inertial frequency of oscillation (f) is resonant with the diurnal period of the solar forcing cycle. The relevance of such "critical latitude" response is difficult to test over North America because of the abrupt change of distribution of land and sea that occurs close to 30° latitude. Over South America, the Andes Mountains and surrounding plains continue unobstructed over a much broader range of latitudes, and the present study supports the importance of the near-resonant response in the vicinity of 30°S as may be inferred from Fig. 10.

5. Conclusions

This study has documented a seesaw pattern on the SACZ with amplitude reversals in approximately 10 days. Events associated with strong convective activity over the SACZ are associated with rainfall deficits over the subtropical plains of South America. In contrast, when the SACZ weakens, precipitation over these plains is abundant. These results are in agreement with those of Kousky and Casarin (1986).

The SASS is found to be a regional component of a larger oscillatory pattern that extends from the date line into the Atlantic and has a meridional extent of approximately 70° in latitude, from about 50°S into the Gulf of Mexico. No explanation is offered here for the causes of this phenomenon, though its timescale suggests a possible link with the 30–60-day intraseasonal oscillation.

The 200-hPa height field depicts a wave pattern with below normal heights off the southwest coast of Chile at about 45°S associated with enhanced precipitation in the subtropical plains of South America. Its wavelength is about 70° longitude, and it spans a region from the mid- to tropical latitudes. Low-level patterns are strongly modified by the Andes Cordillera with strong northerlies to the east of the mountains for wet episodes over the subtropical plains. The 90° lag between circulations at 200- and 850-hPa levels, as well as the horizontal scale of the wave pattern, indicates the active role that low-frequency baroclinic synoptic eddies play for these wet episodes. Nevertheless, the link with tropical convection suggests that explanations for the SASS need

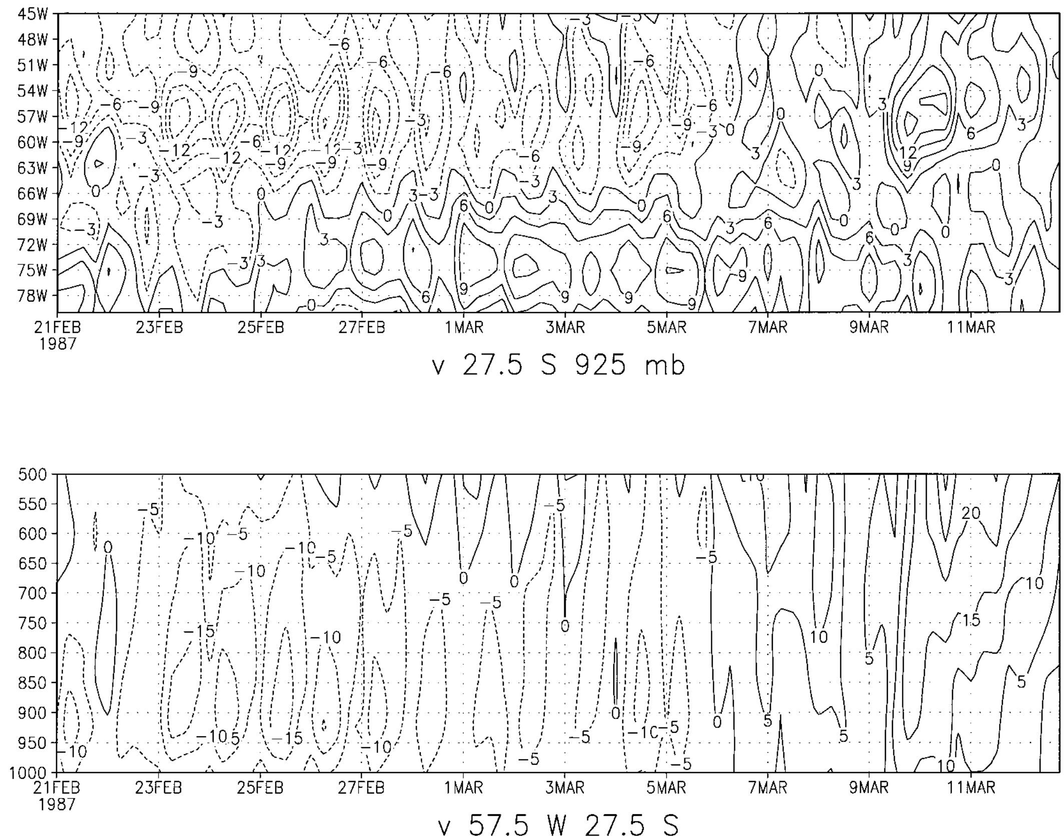

FIG. 14. (top) Longitude–time diagram for meridional wind at 27.5°S, 925-hPa level. Contour interval is 3 m s^{-1}. (bottom) Height–time diagram for the meridional wind at 27.5°S, 57.5°W, contoured every 5 m s^{-1}.

to include tropical as well as extratropical dynamics. In this sense the SACZ associated with a SASS differs considerably from the seasonally averaged pattern shown in Fig. 1, which has been well simulated by regional models centered on tropical South America (Figueroa et al. 1995).

Additionally, we have also documented an influx of moisture from the Tropics into central Argentina and southern Brazil for wet periods there. The moisture influx is caused by a strong LLJ east of the Andes. This result agrees with the findings of Wang and Paegle (1996). The LLJ displays a marked diurnal oscillation, and it appears to have similar characteristics to the well-documented LLJs over the Great Plains of North America (e.g., Paegle et al. 1996). Both the North and South American LLJs play similar roles in establishing moisture corridors that produce rainfall in subtropical and midlatitudes of both continents during the summer. The moisture source is different: the Gulf of Mexico is an unlimited moisture source for the Great Plains of North America, while the northerlies that carry moisture southward east of the Andes over South America originate over land, and its moisture transport capacity depends on the water balance over tropical South America.

Acknowledgments. This investigation was supported by NOAA Grants GC95-013 and GC95-833 to the University of Utah. The interpolated OLR data was kindly provided by B. Liebmann of CIRES/ERL/NOAA.

REFERENCES

Berri, G. J., and B. J. Inzunza, 1993: The effect of the low-level jet on the poleward water vapor transport in the central region of South America. *Atmos. Environ.,* **27A,** 335–341.

Bloom, S. C., L. L. Takacs, and E. Brin, 1991: A scheme to incorporate analysis increments gradually in the GLA assimilation system. *Proc. Ninth Conf. on Numerical Weather Prediction,* Denver, CO, Amer. Meteor. Soc., 110–112.

Buchmann, J., J. Paegle, and L. E. Buja, 1990: The effect of tropical Atlantic heating anomalies upon GCM rain forecasts over the Americas. *J. Climate,* **3,** 189–208.

Figueroa, S., P. Satyamurti, and P. L. Silva Dias, 1995: Simulation of the summer circulation over the South American region with an eta coordinate model. *J. Atmos. Sci.,* **52,** 1573–1584.

Gandu, A. W., and J. E. Geisler, 1991: A primitive equations model study of the effect of topography on the summer circulation over tropical South America. *J. Atmos. Sci.,* **48,** 1822–1836.

Gill, A. E., 1980: Some simple solutions for heat-induced tropical circulation. *Quart. J. Roy. Meteor. Soc.,* **106,** 447–462.

Holton, J. R., 1967: Diurnal boundary layer wind oscillation over sloping terrain. *Tellus,* **19,** 199–205.

Kalnay, E., and Coauthors, 1996: The NCEP/NCAR 40-year reanalysis project. *Bull. Amer. Meteor. Soc.,* **77,** 437–471.

Kleeman, R., 1989: A modeling study of the effect of the Andes on the summer circulation of tropical South America. *J. Atmos. Sci.,* **46,** 3344–3362.

Kousky, V. E., and D. P. Casarin, 1986: Rainfall anomalies in southern Brazil and related atmospheric circulation features. *Extended Abstract, Second Int. Conf. on Southern Hemisphere Meteorology,* Wellington, New Zealand, Amer. Meteor. Soc., 435–438.

——, and M. T. Kayano, 1994: Principal modes of outgoing longwave radiation and 250-mb circulation for the South American sector. *J. Climate,* **7,** 1131–1143.

Liebmann, B., and C. A. Smith, 1996: Description of a complete (interpolated) outgoing longwave radiation dataset. *Bull. Amer. Meteor. Soc.,* **77,** 1275–1277.

Meehl, G. A., 1992: Effect of tropical topography on global climate. *Annu. Rev. Earth Planet. Sci.,* **20,** 85–112.

Mesinger, F., and A. Arakawa, 1976: Numerical methods used in atmospheric models. GARP Publ. 17, 64 pp. [Available from WMO, Case Postale 2300, CH-1211 Geneva 2, Switzerland.]

Mo, K. C., and R. W. Higgins, 1996: Large-scale atmospheric moisture transport as evaluated in the NCEP/NCAR and the NASA/DAO reanalyses. *J. Climate,* **9,** 1531–1545.

Moorthi, S., and M. J. Suarez, 1992: Relaxed Arakawa–Schubert: A parameterization of moist convection for general circulation models. *Mon. Wea. Rev.,* **120,** 978–1002.

O'Lenic, E. A., and R. L. Livezey, 1988: Practical considerations in the use of rotated principal component analysis (RPCA) in diagnostic studies of upper air height fields. *Mon. Wea. Rev.,* **106,** 1682–1689.

Paegle, J., K. C. Mo, and J. N. Paegle, 1996: Dependence of simulated precipitation on surface evaporation during the 1993 United States summer floods. *Mon. Wea. Rev.,* **124,** 345–361.

Pan, H. L., and W. S. Wu, 1993: Implementing a mass flux convection parameterization package for the NMC Medium Range Forecast Model. *Proc. 10th Conf. on Numerical Weather Prediction,* Portland, OR, Amer. Meteor. Soc., 96–99.

Park, C.-K., and S. D. Schubert, 1993: Remotely forced intraseasonal oscillations over the tropical Atlantic. *J. Atmos. Sci.,* **50,** 89–103.

Pfaendtner, J., S. Bloom, D. Lamich, M. Seablom, M. Seinkiewicz, J. Stobie, and A. Da Silva, 1995: Documentation of the Goddard Earth Observing System (GEOS) Data Assimilation System—Version 1. NASA Tech. Memo. 104606, Vol. 4, 44 pp. [Available from Goddard Space Flight Center, Greenbelt, MD 20771.]

Rao, G. V., and S. Ergodan, 1989: The atmospheric heat source over the Bolivian Plateau for a mean January. *Bound.-Layer Meteor.,* **46,** 13–33.

Richman, M. B., 1986: Rotation of principal components. *J. Climatol.,* **6,** 293–335.

——, and P. J. Lamb, 1985: Climatic pattern analysis of three- and seven-day summer rainfall in the central United States: Some methodological considerations and a regionalization. *J. Climate Appl. Meteor.,* **24,** 1325–1343.

Schemm, J. K., S. Schubert, J. Terry, and S. Bloom, 1992: Estimates of monthly mean soil moisture for 1979–89. NASA Tech. Memo. 104571, 252 pp. [Available from Global Modeling and Simulation Branch, Code 911, NASA/GSFC, Greenbelt, MD 20771.]

Schubert, S. D., R. B. Rood, and J. Pfaendtner, 1993: An assimilated dataset for earth applications. *Bull. Amer. Meteor. Soc.,* **74,** 2331–2342.

Sellers, P. J., Y. Mintz, Y. C. Sud, and A. Dalcher, 1986: A simple biosphere model (SIB) for use within general circulation models. *J. Atmos. Sci.,* **43,** 505–531.

Silva Dias, P. L., W. H. Schubert, and M. DeMaria, 1983: Large-scale response of the tropical atmosphere to transient convection. *J. Atmos. Sci.,* **40,** 2689–2707.

Wang, M., and J. Paegle, 1996: Impact of analysis uncertainty upon regional atmospheric moisture flux. *J. Geophys. Res.,* **101,** 7291–7303.